HHS Public Access

Author manuscript

Clin Cancer Res. Author manuscript; available in PMC 2017 March 01.

Published in final edited form as:

Clin Cancer Res. 2016 March 1; 22(5): 1173–1184. doi:10.1158/1078-0432.CCR-15-1352.

PD-1 blockade boosts radiofrequency ablation-elicited adaptive immune responses against tumor

Liangrong Shi[#1,2,3], **Lujun Chen**[#1,3], **Changping Wu**[1,2,3,*], **Yibei Zhu**[4], **Bin Xu**[1,3], **Xiao Zheng**[1,3], **Mingfen Sun**[1,3], **Wen Wen**[4], **Xichao Dai**[1,2,3], **Min Yang**[1,2,3,4], **Quansheng Lv**[4], **Binfeng Lu**[5,*], and **Jingting Jiang**[1,3,*]

[1]Department of Tumor Biological Treatment, Soochow University, Changzhou 213003, Jiangsu, China

[2]Department of Oncology, the Third Affiliated Hospital, Soochow University, Changzhou 213003, Jiangsu, China

[3] Jiangsu Engineering Research Center for tumor Immunotherapy, Changzhou 213003, Jiangsu, China

[4] Institute of Biotechnology, Key Laboratory of Clinical Immunology of Jiangsu Province, Soochow University, Jiangsu Suzhou, China

[5] Department of Immunology, University of Pittsburgh, 200 Lothrop Street, Pittsburgh, PA 15213, USA

[#] These authors contributed equally to this work.

Abstract

Purpose—Radiofrequency ablation (RFA) has been shown to elicit tumor-specific T cell immune responses but is not sufficient to prevent cancer progression. Here we investigated immune suppressive mechanisms limiting the efficacy of RFA.

Experimental design—We performed a retrospective case-controlled study on patients with synchronous colorectal cancer liver metastases who had received primary tumor resection with or without pre-operative RFA for liver metastases. Tumor infiltrating T cells and tumoral PD-L1 expression in human colorectal cancer tissues were analyzed by immunohistochemistry. T cell immune responses and PD-1/PD-L1 expression were also characterized in a RFA mouse model. In addition, the combined effect of RAF and PD-1 blockade was evaluated in the mouse RFA model.

Results—We found that RFA treatment of liver metastases increased not only T cell infiltration but also PD-L1 expression in primary human colorectal tumors. Using mouse tumor models, we demonstrated that RFA treatment of one tumor initially enhanced a strong T cell-mediated

[*]Corresponding authors: Changping Wu, Department of Tumor Biological Treatment, Department of Oncology, the Third Affiliated Hospital, Soochow University, Changzhou 213003, Jiangsu, China. wcpjjt@163.com; Binfeng Lu, Department of Immunology, University of Pittsburgh, 200 Lothrop Street, Pittsburgh, PA 15213, USA. binfeng@pitt.edu; Jingting Jiang, Department of Tumor Biological Treatment, the Third Affiliated Hospital of Soochow University, Changzhou 213003, Jiangsu, China. jiangjingting@suda.edu.cn..

Disclosure

There are no potential conflicts of interest to disclose.

immune response in tumor. Nevertheless, tumor quickly overcame the immune responses by inhibiting the function of $CD8^+$ and $CD4^+$T cells, driving a shift to higher Treg to Teff ratio, and up-regulating of PD-L1/PD-1 expression. Furthermore, we established that the combined therapy of RFA and anti-PD-1 antibodies significantly enhanced T cell immune responses, resulting in stronger antitumor immunity and prolonged survival.

Conclusions—The PD-L1/PD-1 axis plays a critical role in dampening RFA-induced antitumor immune responses. And this study provides a strong rationale for combining RFA and the PD-L1/PD-1 blockade in the clinical setting.

Keywords

Radiofrequency ablation; Programmed death-1; Programmed death ligand-1; Antitumor immunity; Colorectal cancer liver metastases

Introduction

Radiofrequency ablation (RFA) is widely used as a local treatment for tumors such as small hepatocellular carcinomas, renal cancer and solitary colorectal cancer liver metastases (CRCLM) (1-3). RFA induces localized coagulation necrosis and leads to the release of large amounts of cellular debris *in situ*, which can serve as a source of tumor antigens to elicit host adaptive immune responses against tumors (4). Several studies on preclinical animal models have shown that localized tumor ablation by RFA can induce systemic T-cell mediated antitumor immunity (5-7). Antigen-specific T cell immune responses were also observed in patients with hepatic tumors after RFA therapy (8, 9). However, the RFA-induced immune responses are not sufficient to prevent tumor recurrence. The underlying mechanisms remain obscure.

Programmed death-ligand 1 (PD-L1), an important immune checkpoint molecule, is often up-regulated on tumor cells and tumor associated myeloid cells. It impairs T cell-mediated immune responses upon engagement with its cognate co-inhibitory receptor PD-1, which is always highly expressed on tumor-infiltrating lymphocytes (10-12). PD-L1 expression can be induced by pro-inflammatory cytokines, especially type II interferon (IFN), as an important self-limiting mechanism to prevent rampant autoimmunity (11, 13). Recent studies show that PD-L1 expression on tumor cells is associated with T cell infiltration, suggesting PD-L1 is actively involved in suppressing antitumor immune responses in the tumor microenvironment (TME) (13-15). Whether the PD-L1/PD1 axis is involved in modulating the antitumor T cell immune responses induced by RFA is unclear.

The objective of this investigation was to study the RFA-induced immune responses in tumor tissues from cancer patients and tumor-bearing mice. We first examined tumor specimens from a unique cohort of colorectal cancer patients to establish whether RFA induces immune responses against tumor and potential involvement of PD-L1/PD-1 in limiting such immune responses. Mouse models were then used to characterize RFA-induced immune responses and PD-L1/PD-1-mediated immune suppression. Furthermore, the combination therapy of RFA and PD-1 blockade was evaluated. Our studies are designed

to provide new insight into immune suppressive mechanisms limiting RFA efficacy and explore the potential of PD-1 blockade in combination with RFA in cancer therapy.

Methods

Study patients

Patient selection and study: A patient database was queried for all patients having colorectal cancer from Jan 2007 to Dec 2013 at the Third Affiliated Hospital of Soochow University. A total of 391 consecutive patients with synchronous liver metastases (LM) were initially included in this study. Among them, 38 patients who received initial hepatic RFA followed by primary tumor resection were included in the RFA group, while other 40 patients who received initial primary tumor resection were identified as Non-RFA group. The other 313 patients were excluded for: preoperative chemotherapy and/or radiotherapy or other types of cancer treatment (242 patients), emergency surgery for complications related to primary tumor (45 patients), and initial hepatectomy (19 patients). In addition, 7 patients who had no matched endoscopic biopsy specimen were also excluded. Paired preoperative biopsy and resected tumor specimens of all 78 patients included were collected for immunohistochemical (IHC) staining. Clinical data, including age, gender, location of primary tumor and number of LM, were obtained from the database. All resected tumor specimens were reviewed and classified according to the 7th edition of International Union Against Cancer (UICC) TNM staging system. The study design is outlined in Figure S1. This study was conducted according to the principles of the Declaration of Helsinki and was approved by the Ethics Committee of Soochow University.

RFA treatment for colorectal cancer patients with liver metastases

RFA was performed percutaneously under compound anesthesia of vein and guided by ultrasonography (US) or computed tomography (CT). All ablations were performed using the RITA 1500 generator (RITA Medical Systems Inc., Mountain View, CA, USA). This system consists of a 150 Watt generator and a multitined expandable electrode (StarBurst XL, RITA). The multitined expandable electrode consists of a 15-gauge insulated cannula and nine individual electrode tines of 10 to 15 cm in length. It was deployed *in situ* after ultrasound or computed tomography-guided placement of the needle electrode into the target tumor. For tumors less than 3.0 cm in diameter, the multitined expandable electrode was deployed into the center of the tumor. Each application of RFA energy lasted for 15-25 minutes to gain a 5.0 cm ablation zone. For tumors larger than 3.0 cm, multiple overlapping zones of ablation were needed for the destruction of the tumor and a surrounding rim of non-tumor liver. For patients with more than one lesion, the tumors were ablated separately.

Immunohistochemistry procedures and evaluation

Formalin-fixed, paraffin-embedded tissues were processed for immunohistochemical staining with antibodies for PD-L1 (1:500, clone: SP142, Spring Bioscience), which has been used in prior clinical studies (16, 17), CD4 (clone: SP35, Maixin Biotechnology Co), and CD8 (clone: SP16, Maixin Biotechnology Co). The quantification of PD-L1 staining for tumor cells and lymphocytes were completed in 5–10% increments as previously described (14). Positive PD-L1 expression was defined as ≥ 5% cells with membranous staining. An

adjusted score representing PD-L1 expression on lymphocytes was calculated as the percentage of lymphocytes stained positive for PD-L1 multiplied by the extent of lymphocytic infiltration (0 = absent, 1= focal, 2 = moderate, and 3 marked) (18). PD-L1 staining in melanoma and human placenta specimens was used as positive control (Figure S2). The evaluation of the number of TIL has been described previously (19). In brief, tumor infiltrating T cells in tumor nest were counted as follows: five areas in tumor nest with the most intense T lymphocytes infiltration were selected at low magnification (x40), and subsequently counted and recorded at high power field (HPF, x200 magnification). Results from the five areas were averaged and used in the statistical analysis.

Cell lines and cell culture

The mouse colon cancer cell line CT26, the mouse melanoma cancer cell line B16, and the mouse breast cancer cell line 4T1 were obtained from Chinese Academy of Sciences, Shanghai Institutes for Biological Sciences (Shanghai, China).

Animal models and treatments

1×10^6 CT26 or B16 cells were symmetrically injected *i.d.* into male BALB/C and C57BL/6 mice on bilateral flanks, respectively. Treatments were initiated when the tumor volume reached about 500 mm^3. RFA was carried out only for the tumor on the right flank. RFA was performed using a 17-gauge single ablation electrode (RITA Medical Systems Inc., Mountain View, CA, USA) with 1 cm active tip inserted percutaneously and orthogonal to the skin in the center of the tumor. Treatments were administered for 3.5-4.5 minutes at the target temperature of 70°C to ensure complete ablation of the target tumors. PD-1 blockade was accomplished by administering 200 μg anti-PD-1 (clone: J43, BioXCell) through i.p. injection to mice every 3 days for a total of four times. To deplete $CD8^+$ T cell, 250 μg anti-CD8 (clone 2.43; Bio-XCell) was delivered per mouse four times by *i.p.* injection every 3 days, starting from 1 day before RFA. Perpendicular diameters of the tumor on the left flanks were measured using calipers every 3 days. Tumor size was calculated using the formula L×W, where L is the longest dimension and W is the perpendicular dimension.

Flow cytometric analysis

The tumor infiltrating lymphocytes were harvested according to the method described in our previous study (20). In brief, the tumor masses were removed, minced and digested with collagenase and hyaluronidase solution. The cell suspension was filtered through a cell mesh and resuspended in Hank's media plus 1% fetal calf serum (FCS) for further analysis. Antibodies to PD-L1 (MIH5), PD-1 (RPM1-30), CD4 (GK1.5), CD8 (53-6.7), IFN-γ (XMG1.2),TNF-α (MP6-XT22), CD3 (145-2c11), Gr1 (RB6-8C5), CD11b (M1/70), CD45 (30-F11), FOXP3 (FJK-16S), eomes (Dan11mag), CD244 (eBio244F4) and CD160 (eBioALC48) were purchased from eBioscience. F4/80 (BM8), CD11c (N418), and Tim-3 (B8.2C12) antibodies were purchased from Biolegend. Flow cytometric analysis was performed using a FACS flow cytometer (Becton Dickinson). For intracellular cytokine staining, harvested cells were stimulated with PMA (10 ng/ml) and ionomycin (1 μg/ml) for 4 h and incubated for the last one hour with brefeldin A (10 μg/ml). IFN-γ and TNF-α producing cells were examined with flow cytometry.

ELISPOT assay

Elispot assay was performed according to the instructions of the instrument manufacturer and as described before (21). Enzyme-linked immunosorbent spot (ELISPOT) plates (MABTECH AB-plus; Sweden, Product code: 3321-4APT-4) were washed 4 times with sterile PBS (200μl/well) and incubated with medium containing 10% serum for 30 minutes at room temperature. 4T1 breast cancer cells were pulsed with 10 mg/mL of AH1 peptide (SPSYVYHQF) overnight. A total of 10^6 $CD8^+$ T cells isolated from spleen or draining lymph node were plated in quadruplicates to be cocultured with pulsed or non-pulsed 10^5 4T1 cells. These cells were later stimulated with 1 mmol/L of phorbol 12-myristate 13-acetate and 10 ng/mL of Ionomycin as positive controls and with medium alone as negative controls. The plates were incubated in a 37°C humidified incubator with 5% CO_2 for 24 hours. Rat anti-mouse IFN-γ mAb (R4-6A2-biotin, 1μg/mL) was used for detection. After 2-hour incubation with detection antibody, the plates were washed and incubated with Streptavidin-ALP for 1 hour at room temperature. Finally, substrate solution (BCIP/NBT-plus) was added to develop spots and analysis was done using an ELISPOT Plate Reader (iSPOT, German).

Quantitative real-time PCR

The mRNA levels of IFN-γ, TNF-α, PD-1, PD-L1 and the reference gene β-actin were measured by real-time PCR machine, ABI 7500 (Applied Biosystem, USA). In brief, total RNA was extracted from tissues, according to the manufacturer's instructions, using a total RNA purification kit (Shenergy Biocolor BioScience & Technology Company, Shanghai, China). The quality of the RNA was determined by measuring the absorbance at 260/280 nm. Using the first strand cDNA synthesis kit (Fermantas, Vilnius, Lithuania), according to the manufacturer's instructions, 2μg total RNA was reverse transcribed to cDNA. The primers and TaqMan probes of INF-γ, TNF-α, PD-1, PD-L1 and the reference gene β-actin were designed according to the National Center for Biotechnology Information (NCBI) database by using Primer Premier 5.0 software (Palo Alto, CA, USA). The sequences of all primers used in this study are listed in Table S1.

Statistics

Differences in distribution of selected demographic and clinical characteristics between RFA and Non-RFA groups were performed using Student's t-test and Fisher Chi-square test. We examined correlation between PD-L1 expression on tumor cells and intensity of T cell infiltration, using Spearman test. Wilcoxon signed rank test was used to test differences in intensity of T cell infiltration and PD-L1 expression between matched specimens (endoscopic biopsy *vs* resected primary tumor) within RFA and Non-RFA group, respectively. Mann-Whitney U test was used to examine differences between 2 groups. Logistical regression analysis was used to identify potential associated with increase of PD-L1 expression in resected tumor specimens compared to endoscopic biopsy specimens.

Data from animal experiments were expressed as mean ± SEM for biological replicates and mean ± SD for technical replicates. Two-tailed unpaired Student's t-test was used for comparison of 2 groups (RFA-treated mice and control). ANOVA test were used for comparisons of groups in studies involving combinations of RFA with anti-PD-1. Survival

data were analyzed by Log-Rank test. $P < 0.05$ was considered statistically significant. Data were analyzed using SPSS software (Version 13.0, SPSS Inc., Chicago, IL, USA.).

Results

Both the number of tumor infiltrating lymphocytes (TIL) and expression of PD-L1 were increased in the primary tumor upon RFA treatment of colorectal hepatic metastases

It has been shown that RFA induced systemic tumor antigen-specific T cell responses in human carcinoma. However, there are insufficient studies on the immune modulation of TME outside of the ablation zone. In order to study how RFA modifies TME in human cancer patients, we performed a retrospective study of a unique cohort of patients who suffered from synchronous CRCLM. Thirty-eight patients who received preoperative RFA for LM followed by primary tumor resection were assigned to the RFA group, whereas forty patients who received primary tumor resection without RFA were included in the non-RFA group. There was no significant difference in demographic, clinical characteristics and staging between the RFA and non-RFA groups (Table S2). The median time interval from RFA to primary tumor resection was 6 days (range, 4 to 10 days).

We first sought to determine whether RFA induces T cell immune responses in TME using the frequency of $CD4^+$ and $CD8^+$ TIL as an indicator. There was no difference in the number of infiltrating T cells between RFA and non-RFA groups prior to treatment, as shown in results obtained using the endoscopic biopsy (EB) specimens (Mann-Whitney test, P=0.268 for $CD8^+$ T cell, P=0.812 for $CD4^+$ T cell, Table 1). Interestingly, however, a higher number of tumor infiltrating T cells were observed in the RFA group compared to that of the non-RFA group in resected tumors (RT) specimens (Mann-Whitney test, P<0.001 for $CD8^+$ T cell, P=0.001 for $CD4^+$ T cell, Table 1). In addition, the CD8 to CD4 ratio was higher in the RFA group compared to non-RFA group in the RT specimens (Fisher Chi square test, P=0.002, Table 1, Figure 1A, Figure S3). These data indicated that RFA elevated T cell immune responses in TME.

We also compared the intensity of T cell infiltration between matched EB and RT specimens on case by case basis. As shown in a previous study (22), for the non-RFA group, the number of infiltrating T cell in RT specimen was similar to that in EB specimen (Wilcoxon Signed Ranks test, P=0.117 for $CD8^+$ and P=0.754 for $CD4^+$, respectively). In contrast, in the RFA group, the frequency of infiltrating $CD8^+$ and $CD4^+$ T cell was significantly increased in the RT specimens when compared to the EB specimens (Wilcoxon Signed Ranks test, P=0.003 and P=0.002, respectively). In addition, in the RFA group, a higher CD8 to CD4 ratio was found in the RT specimens when compared to the EB specimens (Fisher Chi square test, P=0.002, Figure 1A, Figure S3), consistent with the idea that a strong $CD8^+$ T cell-mediated immune response is promoted by RFA.

We also characterized the PD-L1 expression in tumor tissues because it is an important checkpoint molecule limiting T cell responses. PD-L1 expression was found on both tumor cells and tumor associated immune cells. Among 78 EB specimens, 18 (23.1%) (9 each for the RFA and non-RFA groups) showed positive PD-L1 expression on tumor cells. 31 (39.7%) (14 of the RFA group and 17 of the non-RFA group) showed significant PD-L1

expression on infiltrating immune cells. Among the RT specimens, 25 (32.1%) (15 of RFA group and 10 of Non-RFA group) had PD-L1 expression on tumor cells, whereas 40 (51.3%) (22 of the RFA group and 18 of the non-RFA group) had PD-L1 expression on immune cells. In all groups, levels of PD-L1 expression on tumor cells were significantly associated with PD-L1 expression on immune cells. Both EB and RT specimens showed a significant association between PD-L1 expression on tumor cells and the intensity of $CD8^+$ T infiltration (Spearman correlation, P=0.001 for EB and P<0.001 for RT specimens) (Figure S4A and C). In contrast, there is no significant association between tumor PD-L1 expression and intensity of $CD4^+$ T cell infiltration (Spearman correlation, P=0.159, for EB and P=0.065 for RT specimens) (Figure S4B and D).

We sought to determine whether RFA treatment resulted in changes of PD-L1 expression. In the non-RFA group, PD-L1 expression in the RT specimens was similar to that in the matched EB specimen (Wilcoxon Signed Ranks test, P=0.234 for PD-L1 expression on tumor cells and P=0.194 for that on immune cells, Figure 1B and E). In contrast, within the RFA group, an increase of PD-L1 expression was observed not only on tumor cells but also on immune cells in the RT specimens when compared to matched EB specimens (Wilcoxon Signed Ranks test, P=0.0001 and P=0.0003, respectively) (Figure 1A, C, F, and Figure S3). Interestingly, 78.6% of the cases that were PD-L1 positive at the initial biopsy had increases in PD-L1 expression after RFA. Moreover, 33.3% of the cases that were PD-L1 negative at the initial biopsy became PD-L1 positive for the matched RT specimens after RFA.

In order to more accurately demonstrate the impact of hepatic RFA on the PD-L1 expression in primary tumors, we introduced a new variable “ΔPD-L1” (ΔPD-L1 on tumor cell = percentage of positive cell in the RT specimen - percentage of positive cell in the EB specimen; ΔPD-L1 on immune cell = adjusted IHC score in the RT specimen-IHC score in the EB specimen). This variable also helps control for variations in the baselines that may affect the quantification of PD-L1 expression. ΔPD-L1 on both tumor cells and immune cells were higher in the RFA group than in non-RFA group (Mann-Whitney U test, P=0.0004 and P<0.0001, respectively, Figure 1D and G). In addition, after adjustment for other variables including sex, year, tumor grade, histological type, numbers of LM, the site of primary tumor, regional lymph node status, we revealed a significant association between hepatic RFA and increased PD-L1 expression in primary tumor (OR 25.71, 95%CI: 4.52-146.16, P<0.001, Table S3). Collectively, this suggests that RFA of metastatic tumors induced T cell-mediated immune responses against primary tumor as well as PD-L1 expression as a self-limiting mechanism.

RFA induces modest and short-lived growth inhibition of distant tumors

In order to further study RFA-induced immune responses, mice were inoculated with CT26, a murine colon cancer cell line that has been shown sensitivity to checkpoint blockade (23), on bilateral flanks. RFA was then performed on the tumor at the right flank once the tumor volume reached about 500 mm^3. The growth of the tumor at the left flank was monitored. A slight halt of growth of the contralateral tumor was observed after the RFA. However, on around days 6 to 9, the contralateral tumor restored its progressive growth (Figure 2A). We also confirmed this finding with the B16 melanoma model (Figure 2B).

Infiltrating T cells in the distant tumor displayed a potent but transient antitumor effector function, which waned as the tumor regained its growth

To better understand the magnitude and duration of antitumor immune responses induced by RFA, we performed immune analysis at an earlier and later time points in the distant CT26 tumor after RFA treatment. On day 3, about two-fold increase of the percentage of the $CD45^+$ immune cells was observed in the distant tumor of the RFA-treated mice. Interestingly, the frequency of $CD45^+$ infiltrating cells increased further on day 8 (Figure S5A-C). This indicated that localized tumor ablation induced a sustained inflammatory response in the distant tumor even at a later stage when tumor had restored rapid growth. The T cell infiltration was characterized by increased frequencies of $CD4^+$ and $CD8^+$ T cells on day 3 and 8 (Figure 3A-C, Figure S5D and E). The percentage of Treg was reduced in RFA-treated mice on day 3 (Figure 3D and E). This resulted in an increase in the ratio of CD8 vs Treg (Figure 3F), indicating a shift of immune balance towards antitumor immunity on day 3 upon RFA. However, the shift was temporary. On day 8, the percentage of Treg was at a similar level to that in the untreated mice (Figure 3D and E). On day 8 after RFA, The $CD8^+$ T cell to Treg ratio was significantly decreased as comparing to that on day 3 ($P<0.001$), whereas it was still modestly higher due to an increase in $CD8^+$ T cell infiltration (Figure 3F). Similar results were obtained using B16 melanoma tumor model (Figure S6A-G). These results suggest that an antitumor immune response is induced by RFA but is tamed by the active immune suppression in TME.

In order to determine the function of TIL, we analyzed the ability of T cells to produce IFN-γ and TNF-α by flow cytometry. On day 3, the percentage of IFN-γ^+ and TNF-α^+ $CD8^+$ TIL was significantly increased in RFA-treated mice when compared to untreated mice. However, the percentage of IFN-γ^+ and TNF-α^+ $CD8^+$TIL was markedly decreased on day 8 and was similar to that in the untreated mice (Figure 3G and H). Similar results were observed on $CD4^+$ TIL (Figure 3G and I). In addition, IFN-γ and TNF-α mRNA expression in tumors were four to five fold higher in RFA-treated mice compared to untreated mice on day 3 (Figure 3J and K). In contrast, IFN-γ and TNF-α mRNA levels were sharply decreased on day 8 (Figure 3J and K). These data indicate that TIL underwent functional exhaustion at the later stage after RFA when tumor regression was reversed.

Expression of PD-L1 and PD-1 in the distant tumor upon RFA treatment

Our data showed that both the number of TIL and expression of PD-L1 were increased in the human primary tumor upon RFA of colorectal hepatic metastases. Here, we sought to examine PD-L1 expression in the TME in CT26 mouse colon cancer model. On day 3, a rapid up-regulation of PD-L1 expression was observed on $CD45^-$ cells isolated from tumor tissues. The proportion of PD-$L1^+CD45^-$ cells increased from about 10% to 23% (Figure 4A and B). Similarly, PD-L1 expression increased in tumor associated DCs, MDSCs and macrophages upon RFA (Figure 4A and B). On day 8, we observed a further increase of PD-L1 expression on all cell populations in the RFA group (Figure 4A and C). In contrast, we did not detect PD-L1 expression on splenic $CD11c^+$, $F4/80^+$ and $CD11b^+Gr1^+$ cells (Figure S7A). In addition, we showed that RFA treatment also led to an increase in PD-L1 expression in B16 tumor tissues (Figure S6H-J). These data indicate that the tumor

inflammatory microenvironment induced by RFA plays a direct role in the up-regulation of PD-L1 expression.

Further analysis showed that approximately 70% of $CD8^+$ and 40% of $CD4^+$ TIL expressed PD-1 in untreated CT26 tumor-bearing mice. On day 3 after RFA, we observed about a 20% decrease in PD-1^+CD8^+ TIL cells compared to those in the untreated mice. However, the frequency of PD-1^+ $CD8^+$ TIL cells increased to more than 80% on day 8 in RFA-treated mice and was slightly higher than those in the untreated mice (Figure 4D and E). The PD-1 expression on $CD4^+$ T cells, however, showed no difference between two groups on both day 3 and 8 (Figure 4F). We did not detect large numbers of PD-1^+ splenic $CD4^+$ and $CD8^+$ T cells on both day 3 and 8 (Figure S7B and C). In B16 tumor, we detected a slight but statistically significant increase of PD-1 expression on both $CD4^+$ and $CD8^+$ TIL on day 8 after RFA (Figure S6K-N).

Our data also showed a significant increase in PD-L1 mRNA in $CD45^-$ cells and total tumors on both day 3 and 8 in CT26 tumor (Figure 4G). The mRNA level of PD-1 in total tumor had no significant change on day 3 after RFA, but increased three fold on day 8 (Figure 4H). In accordance with PD-1 protein expression on $CD8^+$ TIL, PD-1 mRNA also decreased significantly on day 3 and then increased on day 8 in the $CD8^+$ TIL population in the RFA group compared to the non-RFA group (Figure 4H). Collectively, these data suggest that the PD-L1/PD-1 axis is involved in limiting the efficacy of RFA treatment through immune suppression.

In addition, we found that Tim-3, CD160, CD244 and eomes, which are typical exhaustion markers (24), were expressed at higher levels on both $CD8^+$ and $CD4^+$ TIL 8 days after RFA treatment (Figure S8A-F). In contrast, only CD160 and CD244 were expressed at higher levels on day 3 in the RFA group compared to the control. Therefore, in addition to the PD-L1/PD-1 axis, other markers of T cell exhaustion were also induced to higher levels upon RFA treatment.

The combination of RFA and anti-PD-1-treatment synergistically inhibited the growth of the distant tumor through $CD8^+$ T cells

It has been demonstrated that the efficacy of the PD-1 blockade therapy is closely associated with pre-existing tumor antigen-specific T cell immune responses (16, 25). Because RFA induced T cell accumulation and upregulated PD-L1 expression in distant tumor tissues, we postulated that subsequent anti-PD-1 therapy would generate a stronger antitumor immunity and improve the treatment efficacy of RFA. To test the hypothesis, CT26-bearing mice were treated with RFA plus an isotype control antibody, RFA plus anti-PD-1 monoclonal antibodies (mAbs) (RFA+α-PD-1), anti-PD-1 mAbs alone (α-PD-1), or left without treatment (Figure 5A). Because $CD8^+$TIL were significantly increased in tumors after RFA treatment, we also sought to determine whether $CD8^+$ T cells mediate the effect of RFA and PD-1 blockade using CD8-depleting mAbs. No recurrence occurred in the ablation zone. RFA had a modest inhibitory effect on contralateral tumor progression. Anti-PD-1 itself also led to a modest inhibition of tumor growth, consistent with a previous observation (23). In contrast, we observed significant tumor regression, much longer duration of inhibition of tumor growth and prolonged survival in the RFA/anti-PD-1 treated mice, as compared to

mice in the no-treatment or single treatment groups (Figure 5B and C). Depletion of $CD8^+$ T cells completely eliminated the inhibition of tumor growth of mice with the combined treatment (Figure 5B and C). These data indicate that RFA and PD-1 blockade further enhance $CD8^+$ T cell-mediated antitumor immunity.

Combination of RFA and anti-PD-1 mAbs administration further enhanced tumor antigen-specific T cell responses and increased Teff to Treg ratio in the distant tumor

To better determine synergistic antitumor immune responses of the combination of RFA and anti-PD-1, we examined the T cell response in mice treated with RFA, α-PD-1, RFA, RFA +α-PD-1 and no treatment. On day 12, the frequency of both $CD45^+$ and $CD8^+$ cells was higher in RFA-treated and α-PD-1 mAbs-treated mice than in untreated mice (Figure 5D-F, Figure S9A and B). In the RFA plus α-PD-1 mAbs group, the infiltrating $CD45^+$ and $CD8^+$ cell was increased as compared to the RFA or α-PD-1 alone (Figure 5D-F, Figure S9A and B). Importantly, the percentage of IFN-γ^+ and TNF-α^+ $CD8^+$TIL in the RFA plus α-PD-1 mAbs-treated mice increased three fold more than the RFA-treated mice and two fold more than α-PD-1 mAbs-treated mice (Figure 5G and H). Meanwhile, the number of $CD4^+$ TIL and the percentage of IFN-γ^+ and TNFα^+ $CD4^+$TIL were increased in mice receiving combined therapy (Figure 5G, I, and Figure S9C). Quantitative real-time PCR analysis showed that mRNA levels of IFN-γ and TNF-α in contralateral tumor were significantly elevated in the RFA plus α-PD-1-treated mice when compared to the RFA or the α-PD-1 treatment alone groups (Figure 5J). These data suggest that blockade of PD-L1/PD-1 pathway boosted RFA-induced antitumor immune responses and reversed immune suppression at the distant tumor site.

To explore whether systemic tumor-antigen-specific T cells can be induced to a higher level after the combined treatment, we carried out ELISPOT assays for IFN-γ secretion upon ex-vivo re-stimulation of T cells with tumor antigens. $CD8^+$ T cells isolated from spleens and draining lymph nodes (DLNs) were co-cultured with AH1 peptide pulsed with antigen presenting cells (APC). Consistent with the increased number of $CD8^+$ T cells producing IFN-γ in tumor, we detected a significant increase in the number of tumor antigen-specific IFN-γ-secreting cells in both spleens and DLNs from the RFA/α-PD-1-treated mice compared with the RFA or the α-PD-1-treatment alone groups (Figure 5K). Thus, these data indicated that RFA and anti-PD-1 therapy synergistically induced adaptive tumor-antigen-specific $CD8^+$ T cell immune responses.

The PD-L1/PD-1 pathway has been shown to be required for the abundance of Treg in the tumor sites. To assess the impact of PD-1 blockade on the balance between intratumoral Teff and Treg, we examined $CD4^+$FoxP3$^+$Treg in contralateral tumor on day 12 after RFA. Our data showed that the proportion of intra-tumoral Treg was significantly decreased both in mice treated with RFA/anti-PD-1 and anti-PD-1 alone, leading to dramatically elevated $CD8^+$ T cell to Treg ratio as compared to the RFA-treated mice or anti-PD-1-treated mice (Figure 5L-N). Collectively, these data suggest anti-PD-1 therapy reverses adaptive immunosuppression in the distant tumor through reducing Treg and increasing functional effector T cells.

Besides PD1, multiple pathways have been found to be involved in TIL exhaustion (24). In particular, we and others have found that Tim-3 was highly induced in $CD4^+$ and $CD8^+$ TIL in both mouse and human tumors (26-28). Interestingly, we observed a significant increase of Tim-3 on both $CD8^+$ and $CD4^+$ TIL upon PD1 blockade, RFA treatment, or combination treatment (Figure S10A-D). These data suggest that additional regulatory pathways such as Tim-3 might compensate for the lack of PD1 to induce TIL exhaustion.

Discussion

In this study, we have shown that localized RFA increases T cell infiltration as well as PD-L1 expression in a distant tumor in both human patients with synchronous colorectal cancer liver metastases and tumor-bearing mice. Furthermore, using a mouse model, we demonstrated that combination of localized RFA and anti-PD-1 antibodies significantly enhanced tumor antigen-specific T cell responses, increased intratumoral Teff to Treg ratio, and synergistically inhibited growth of the distant tumor.

It has been shown that RFA induced systemic tumor-antigen T cell immune responses in human hepatocellular carcinoma (8, 9). However, these studies are limited to the analysis of peripheral immune cells but not in TME. Due to extensive application of RFA in CRCLM (2) and promotion of “liver first” treatment modality (initial liver resection/ablation followed by primary tumor resection) in resectable synchronous CRCLM (29), we could obtain matched tumor specimens outside of the ablation zone (primary colorectal tumors) prior-RFA (endoscopic biopsy) and post-RFA (resected tumor). Using this novel clinical study design, we revealed a significant increase in T cell infiltration and a higher CD8 to CD4 ratio in the primary colorectal tumor tissues after RFA for liver metastases. These data clearly demonstrated that the localized RFA induced T cell-mediated immune responses in a distant tumor site in human carcinoma. However, RFA is not sufficient to prevent tumor recurrence in clinic, suggesting that duration and function of RFA-induced tumor-specific T cells are inadequate. In this study, we showed that local RFA led to a small and short-lived inhibition of distant tumors in mouse models. We further showed that frequency of IFN-γ and TNF-α-producing $CD8^+$ TIL increased at the early stage after RFA but diminished overtime. In addition, we found that the PD-L1/PD-1 axis plays an important role in mediating suppression of RFA-induced antitumor immunity. Besides PD-L1 and PD-1, CTLA-4 has been shown to inhibit thermal ablation-induced antitumor activities (4, 30, 31). Besides immune inhibitory pathways, it has been shown that various cytokines that are used to enhance T cell homeostasis and T cell immune responses also increase the antitumor efficacy of RFA (32, 33). Thus future combination therapy with RFA and various immune modulators can be explored in the clinical setting.

The abscopal effect we observed with RFA has been described in other tumor therapies. Notebly, radiotherapy has been recently shown to induce similar antitumor effect through induction of tumor antigen specific adative immune responses (34, 35). Blockade of immune checkpoints has been shown to improve the efficacy of radiotherapy on local and distant tumors in experimental systems and as well as in clinical settings (36-38). In a recent report, Victor et al showed a phase I clinical trial of 22 patients with advanced melanoma treated with radiotherapy and anti-CTLA-4 (39). They also found radiotherapy combined with anti-

CTLA-4 enhanced anti-tumor immunity but did not prevent T cell exhaustion in melanoma tumor mouse model. Similar to our study, PD-L1 blockade reversed T-cell exhaustion, promoted T-cell expansion, mitigate depression in the CD8/Treg ratio and led to an optimal response in their preclinical model. Despite similarity between RFA and radiotherapy in the final outcome of induction of adaptive immunity against tumor antigens, the underlying mechanisms could differ. A recent study showed that STING but not MyD88 or TRIF is essential for radiotherapy and the cGAS-STING axis mediates innate sensing of irradiated-tumor cells (40). It remains elusive what triggers innate immunity and set off adaptive immunity in the setting of RFA and the underlying mechanism warrants further studies.

Blockade of the PD-L1/PD-1 axis has achieved remarkable efficacy in clinical trials (17, 41-45). Nevertheless, most patients who lack PD-L1 expression do not benefit from the anti-PD-1 therapy (42), suggesting that efficacy of the anti-PD-1 therapy is closely associated with pre-existing antitumor immune responses (16, 25, 46). Thus, rational combination of treatments that can induce antitumor immune responses and the anti-PD-L1/PD-1 therapy should greatly increase the number of suitable cancer patients. Recently, combining of radiotherapy and PD-L1/PD-1 blockade have been shown to synergistically enhance antitumor immunity in preclinical studies (36, 47, 48), suggesting local antitumor treatments which can elicit immune response hold promise in providing opportunity for PD-1/PD-L1 blockade therapy.

Taube et al have shown that the PD-L1 expression in CRC was relatively lower in contrast to other cancer types such as melanoma, kidney cancer and lung cancer *etc* (46). In this study, we also revealed a low frequency of PD-L1 expression. Interestingly, we demonstrated that RFA for liver metastases up-regulated PD-L1 expression which is associated with an increase in T cell infiltration in primary colorectal cancer. On one hand, these findings indicate that RFA-stimulated antitumor immune responses are dampened by PD-L1. On the other hand, our studies strongly suggest that RFA increases the number of patients that can potentially benefit from the powerful anti-PD-L1/PD-1 therapy.

There are several potential advantages of combining RFA and the PD-L1/PD-1 blockade. Firstly, RFA is widely used in CRCLM (49), making it feasible to explore its role in a novel combined modality. Secondly, RFA results in the instant release of large amounts of tumor antigens in the milieu of “danger” signals, which can potentially stimulate transient immune responses to a wide of variety of tumor antigens. Third, the PD-1 mAbs treatment has shown promising results in CRC in a phase I clinical trial (45) and a study showed that the microsatellite instable subset of CRC can be a good candidate for checkpoint blockade immunotherapy (50). Thus, these results and our study strongly support combining RFA and blockade of the PD-L1/PD-1 for the treatment of metastatic CRC patients.

Supplementary Material

Refer to Web version on PubMed Central for supplementary material.

Acknowledgements

This work was supported by grants from the National Natural Science Foundation of China (No.30972703, 81171653, 81201741, 31428005, 31570877, 31570908 and 81301960). The project was also supported by the National Institutes of Health through grants (No. R21CA167229, UL1 RR024153, UL1TR000005, 1P50 CA097190), Roswell Park Cancer Institute/University of Pittsburgh Cancer Institute Ovarian Cancer Specialized Programs of Research Excellence Grants (P50CA159981) and the Key R&D Projects of Science and Technology Department of Jiangsu Province (BE2015633 and BE2015634).

Reference

1. Duan C, Liu M, Zhang Z, Ma K, Bie P. Radiofrequency ablation versus hepatic resection for the treatment of early-stage hepatocellular carcinoma meeting Milan criteria: a systematic review and meta-analysis. World J Surg Oncol. 2013; 11:190. [PubMed: 23941614]
2. Solbiati L, Ahmed M, Cova L, Ierace T, Brioschi M, Goldberg SN. Small liver colorectal metastases treated with percutaneous radiofrequency ablation: local response rate and long-term survival with up to 10-year follow-up. Radiology. 2012; 265:958–68. [PubMed: 23091175]
3. Popovic P, Lukic S, Mijailovic M, Salapura V, Garbajs M, Surlan Popovic K. Percutaneous radiofrequency ablation of small renal cell carcinoma: technique, complications, and outcomes. J BUON. 2012; 17:621–6. [PubMed: 23335516]
4. den Brok MH, Sutmuller RP, van der Voort R, Bennink EJ, Figdor CG, Ruers TJ, et al. In situ tumor ablation creates an antigen source for the generation of antitumor immunity. Cancer Res. 2004; 64:4024–9. [PubMed: 15173017]
5. Wissniowski TT, Hansler J, Neureiter D, Frieser M, Schaber S, Esslinger B, et al. Activation of tumor-specific T lymphocytes by radio-frequency ablation of the VX2 hepatoma in rabbits. Cancer Res. 2003; 63:6496–500. [PubMed: 14559842]
6. Dromi SA, Walsh MP, Herby S, Traughber B, Xie J, Sharma KV, et al. Radiofrequency ablation induces antigen-presenting cell infiltration and amplification of weak tumor-induced immunity. Radiology. 2009; 251:58–66. [PubMed: 19251937]
7. Lin WX, Fifis T, Malcontenti-Wilson C, Nikfarjam M, Muralidharan V, Nguyen L, et al. Induction of Th1Immune responses following laser ablation in a murine model of colorectal liver metastases. J Transl Med. 2011; 9:83. [PubMed: 21619693]
8. Mizukoshi E, Yamashita T, Arai K, Sunagozaka H, Ueda T, Arihara F, et al. Enhancement of tumor-associated antigen-specific T cell responses by radiofrequency ablation of hepatocellular carcinoma. Hepatology. 2013; 57:1448–57. [PubMed: 23174905]
9. Nobuoka D, Motomura Y, Shirakawa H, Yoshikawa T, Kuronuma T, Takahashi M, et al. Radiofrequency ablation for hepatocellular carcinoma induces glypican-3 peptide-specific cytotoxic T lymphocytes. Int J Oncol. 2012; 40:63–70. [PubMed: 21922136]
10. Dong H, Zhu G, Tamada K, Chen L. B7-H1, a third member of the B7 family, co-stimulates T-cell proliferation and interleukin-10 secretion. Nat Med. 1999; 5:1365–9. [PubMed: 10581077]
11. Zou W, Chen L. Inhibitory B7-family molecules in the tumour microenvironment. Nat Rev Immunol. 2008; 8:467–77. [PubMed: 18500231]
12. Dong H, Strome SE, Salomao DR, Tamura H, Hirano F, Flies DB, et al. Tumor-associated B7-H1 promotes T-cell apoptosis: a potential mechanism of immune evasion. Nat Med. 2002; 8:793–800. [PubMed: 12091876]
13. Spranger S, Spaapen RM, Zha Y, Williams J, Meng Y, Ha TT, et al. Up-regulation of PD-L1, IDO, and T(regs) in the melanoma tumor microenvironment is driven by CD8(+) T cells. Sci Transl Med. 2013; 5:200ra116.
14. Taube JM, Anders RA, Young GD, Xu H, Sharma R, McMiller TL, et al. Colocalization of inflammatory response with B7-h1 expression in human melanocytic lesions supports an adaptive resistance mechanism of immune escape. Sci Transl Med. 2012; 4:127ra37.
15. McGray AJ, Hallett R, Bernard D, Swift SL, Zhu Z, Teoderascu F, et al. Immunotherapy-induced CD8+ T cells instigate immune suppression in the tumor. Mol Ther. 2014; 22:206–18. [PubMed: 24196579]

16. Herbst RS, Soria JC, Kowanetz M, Fine GD, Hamid O, Gordon MS, et al. Predictive correlates of response to the anti-PD-L1 antibody MPDL3280A in cancer patients. Nature. 2014; 515:563–7. [PubMed: 25428504]
17. Powles T, Eder JP, Fine GD, Braiteh FS, Loriot Y, Cruz C, et al. MPDL3280A (anti-PD-L1) treatment leads to clinical activity in metastatic bladder cancer. Nature. 2014; 515:558–62. [PubMed: 25428503]
18. Thompson RH, Gillett MD, Cheville JC, Lohse CM, Dong H, Webster WS, et al. Costimulatory B7-H1 in renal cell carcinoma patients: Indicator of tumor aggressiveness and potential therapeutic target. Proc Natl Acad Sci U S A. 2004; 101:17174–9. [PubMed: 15569934]
19. Jing S, Lujun C, Guangbo Z, Jingting J, Ming Z, Yan T, et al. Clinical significance and regulation of the costimulatory molecule B7-H3 in human colorectal carcinoma. Cancer Immunol Immunother. 2010; 59:1163–71. [PubMed: 20333377]
20. Zhu Y, Ju S, Chen E, Dai S, Li C, Morel P, et al. T-bet and eomesodermin are required for T cell-mediated antitumor immune responses. J Immunol. 2010; 185:3174–83. [PubMed: 20713880]
21. Davis MB, Vasquez-Dunddel D, Fu J, Albesiano E, Pardoll D, Kim YJ. Intratumoral administration of TLR4 agonist absorbed into a cellular vector improves antitumor responses. Clin Cancer Res. 2011; 17:3984–92. [PubMed: 21543518]
22. Koelzer VH, Lugli A, Dawson H, Hadrich M, Berger MD, Borner M, et al. CD8/CD45RO T-cell infiltration in endoscopic biopsies of colorectal cancer predicts nodal metastasis and survival. J Transl Med. 2014; 12:81. [PubMed: 24679169]
23. Selby MJ, Engelhardt JJ, Quigley M, Henning KA, Chen T, Srinivasan M, et al. Anti-CTLA-4 antibodies of IgG2a isotype enhance antitumor activity through reduction of intratumoral regulatory T cells. Cancer immunology research. 2013; 1:32–42. [PubMed: 24777248]
24. Wherry EJ, Kurachi M. Molecular and cellular insights into T cell exhaustion. Nat Rev Immunol. 2015; 15:486–99. [PubMed: 26205583]
25. Tumeh PC, Harview CL, Yearley JH, Shintaku IP, Taylor EJ, Robert L, et al. PD-1 blockade induces responses by inhibiting adaptive immune resistance. Nature. 2014; 515:568–71. [PubMed: 25428505]
26. Fourcade J, Sun Z, Benallaoua M, Guillaume P, Luescher IF, Sander C, et al. Upregulation of Tim-3 and PD-1 expression is associated with tumor antigen-specific CD8+ T cell dysfunction in melanoma patients. The Journal of experimental medicine. 2010; 207:2175–86. [PubMed: 20819923]
27. Gao X, Zhu Y, Li G, Huang H, Zhang G, Wang F, et al. TIM-3 expression characterizes regulatory T cells in tumor tissues and is associated with lung cancer progression. PloS one. 2012; 7:e30676. [PubMed: 22363469]
28. Sakuishi K, Apetoh L, Sullivan JM, Blazar BR, Kuchroo VK, Anderson AC. Targeting Tim-3 and PD-1 pathways to reverse T cell exhaustion and restore anti-tumor immunity. The Journal of experimental medicine. 2010; 207:2187–94. [PubMed: 20819927]
29. de Jong MC, van Dam RM, Maas M, Bemelmans MH, Olde Damink SW, Beets GL, et al. The liver-first approach for synchronous colorectal liver metastasis: a 5-year single-centre experience. HPB (Oxford). 2011; 13:745–52. [PubMed: 21929676]
30. den Brok MH, Sutmuller RP, Nierkens S, Bennink EJ, Frielink C, Toonen LW, et al. Efficient loading of dendritic cells following cryo and radiofrequency ablation in combination with immune modulation induces anti-tumour immunity. Br J Cancer. 2006; 95:896–905. [PubMed: 16953240]
31. Waitz R, Solomon SB, Petre EN, Trumble AE, Fasso M, Norton L, et al. Potent induction of tumor immunity by combining tumor cryoablation with anti-CTLA-4 therapy. Cancer Res. 2012; 72:430–9. [PubMed: 22108823]
32. Johnson EE, Yamane BH, Buhtoiarov IN, Lum HD, Rakhmilevich AL, Mahvi DM, et al. Radiofrequency ablation combined with KS-IL2 immunocytokine (EMD 273066) results in an enhanced antitumor effect against murine colon adenocarcinoma. Clin Cancer Res. 2009; 15:4875–84. [PubMed: 19638464]
33. Iida N, Nakamoto Y, Baba T, Nakagawa H, Mizukoshi E, Naito M, et al. Antitumor effect after radiofrequency ablation of murine hepatoma is augmented by an active variant of CC Chemokine

ligand 3/macrophage inflammatory protein-1alpha. Cancer Res. 2010; 70:6556–65. [PubMed: 20663902]

34. Apetoh L, Ghiringhelli F, Tesniere A, Obeid M, Ortiz C, Criollo A, et al. Toll-like receptor 4-dependent contribution of the immune system to anticancer chemotherapy and radiotherapy. Nat Med. 2007; 13:1050–9. [PubMed: 17704786]
35. Lee Y, Auh SL, Wang Y, Burnette B, Meng Y, Beckett M, et al. Therapeutic effects of ablative radiation on local tumor require CD8+ T cells: changing strategies for cancer treatment. Blood. 2009; 114:589–95. [PubMed: 19349616]
36. Deng L, Liang H, Burnette B, Beckett M, Darga T, Weichselbaum RR, et al. Irradiation and anti-PD-L1 treatment synergistically promote antitumor immunity in mice. J Clin Invest. 2014; 124:687–95. [PubMed: 24382348]
37. Postow MA, Callahan MK, Barker CA, Yamada Y, Yuan J, Kitano S, et al. Immunologic correlates of the abscopal effect in a patient with melanoma. N Engl J Med. 2012; 366:925–31. [PubMed: 22397654]
38. Verbrugge I, Hagekyriakou J, Sharp LL, Galli M, West A, McLaughlin NM, et al. Radiotherapy increases the permissiveness of established mammary tumors to rejection by immunomodulatory antibodies. Cancer Res. 2012; 72:3163–74. [PubMed: 22570253]
39. Twyman-Saint Victor C, Rech AJ, Maity A, Rengan R, Pauken KE, Stelekati E, et al. Radiation and dual checkpoint blockade activate non-redundant immune mechanisms in cancer. Nature. 2015; 520:373–7. [PubMed: 25754329]
40. Deng L, Liang H, Xu M, Yang X, Burnette B, Arina A, et al. STING-Dependent Cytosolic DNA Sensing Promotes Radiation-Induced Type I Interferon-Dependent Antitumor Immunity in Immunogenic Tumors. Immunity. 2014; 41:843–52. [PubMed: 25517616]
41. Hamid O, Robert C, Daud A, Hodi FS, Hwu WJ, Kefford R, et al. Safety and tumor responses with lambrolizumab (anti-PD-1) in melanoma. N Engl J Med. 2013; 369:134–44. [PubMed: 23724846]
42. Topalian SL, Hodi FS, Brahmer JR, Gettinger SN, Smith DC, McDermott DF, et al. Safety, activity, and immune correlates of anti-PD-1 antibody in cancer. N Engl J Med. 2012; 366:2443–54. [PubMed: 22658127]
43. Ribas A. Tumor immunotherapy directed at PD-1. N Engl J Med. 2012; 366:2517–9. [PubMed: 22658126]
44. Topalian SL, Sznol M, McDermott DF, Kluger HM, Carvajal RD, Sharfman WH, et al. Survival, durable tumor remission, and long-term safety in patients with advanced melanoma receiving nivolumab. J Clin Oncol. 2014; 32:1020–30. [PubMed: 24590637]
45. Lipson EJ, Sharfman WH, Drake CG, Wollner I, Taube JM, Anders RA, et al. Durable cancer regression off-treatment and effective reinduction therapy with an anti-PD-1 antibody. Clin Cancer Res. 2013; 19:462–8. [PubMed: 23169436]
46. Taube JM, Klein A, Brahmer JR, Xu H, Pan X, Kim JH, et al. Association of PD-1, PD-1 Ligands, and Other Features of the Tumor Immune Microenvironment with Response to Anti-PD-1 Therapy. Clin Cancer Res. 2014; 20:5064–74. [PubMed: 24714771]
47. Dovedi SJ, Adlard AL, Lipowska-Bhalla G, McKenna C, Jones S, Cheadle EJ, et al. Acquired resistance to fractionated radiotherapy can be overcome by concurrent PD-L1 blockade. Cancer Res. 2014; 74:5458–68. [PubMed: 25274032]
48. Victor CT, Rech AJ, Maity A, Rengan R, Pauken KE, Stelekati E, et al. Radiation and dual checkpoint blockade activate non-redundant immune mechanisms in cancer. Nature. 2015
49. Wong SL, Mangu PB, Choti MA, Crocenzi TS, Dodd GD 3rd, Dorfman GS, et al. American Society of Clinical Oncology 2009 clinical evidence review on radiofrequency ablation of hepatic metastases from colorectal cancer. J Clin Oncol. 2010; 28:493–508. [PubMed: 19841322]
50. Xiao Y, Freeman GJ. The microsatellite instable subset of colorectal cancer is a particularly good candidate for checkpoint blockade immunotherapy. Cancer Discov. 2015; 5:16–8. [PubMed: 25583798]

Translational Relevance

Accumulating evidence suggests that efficacy of the anti-PD-1 therapy is closely associated with pre-existing antitumor immune responses. Therefore, eliciting tumor specific T cell immune responses should synergize with current “checkpoint” therapies. We first demonstrated RFA increased T cell infiltration as well as PD-L1 expression in tumor microenvironment in a unique cohort of patients with synchronous colorectal cancer liver metastases. Using mouse tumor models, we demonstrated that the PD-L1/PD-1 axis was involved in limiting RFA-elicited T cell immune responses. The combined therapy of RFA and PD-1 blockade synergistically enhanced T cell-mediated immune responses and tumor rejection. Our data provide a strong rationale for combining RFA and the PD-L1/PD-1 blockade therapy in the clinical setting.

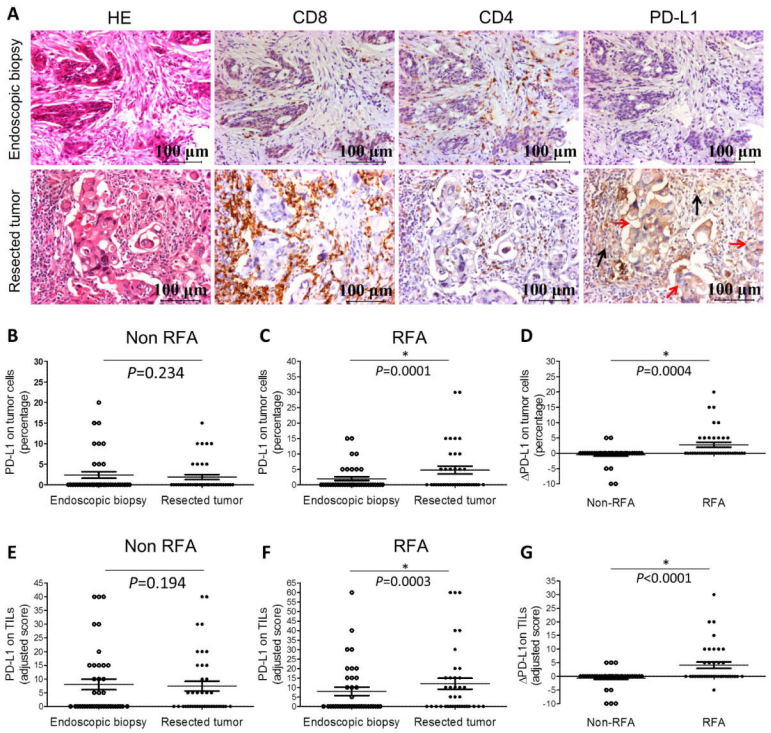

Figure 1. Both the number of TIL and expression of PD-L1 are increased in the primary tumor upon RFA of colorectal liver metastases

A Representative microphotographs showing H&E, CD8, CD4 and PD-L1 staining of matched endoscopic biopsy (top) and resected tumor specimens (bottom). Top row shows $CD8^+$ and $CD4^+$ cells infiltrations and negative PD-L1 expression in EB specimen (X 200); bottom row shows increased infiltration of $CD8^+$, higher CD8 to CD4 ratio and positive PD-L1 expression on immune cells (black arrow) and tumor cells (red arrow) in RT specimen that was obtained 9 days after hepatic RFA. **B** The percentage of PD-L1 membranous expression on tumor cells in matched endoscopic biopsy (EB) and resected tumor (RT) specimens in the non-RFA group. **C** The percentage of PD-L1 membranous expression on tumor cells in the RFA group. **D** ΔPD-L1 on tumor cells (ΔPD-L1 = percentage of tumor cell expressing PD-L1 in RT specimen - percentage of tumor cells expressing PD-L1 in EB specimen) in Non-RFA and RFA group. **E** Adjusted score of PD-L1 expression on infiltrating immune cells in EB and RT specimen in the non-RFA group. **F** Adjusted score of PD-L1 expression on infiltrating immune cells in the RFA group. **G** ΔPD-L1 on immune cells (ΔPD-L1 = adjusted scores in RT specimen - adjusted scores in EB specimen). Wilcoxon Signed Ranks test was used in **B**, **C**, **E** and **F**. Mann-Whitney U test was used in **D** and **G**.

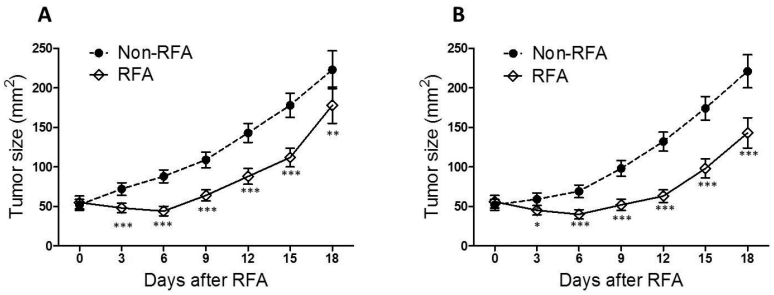

Figure 2. RFA induces slight and short-lived inhibition of distant tumor

1×10^6 CT26 or B16 cells were injected *i.d.* into male BALB/C and C57BL/6 mice, respectively, on bilateral flanks symmetrically. Radiofrequency ablation (RFA) was administrated for the right tumor when the tumor volume reached about 500 mm^3. The size of the left tumor was measured every three days after RFA. **A** Representative data from the CT26 model. **B** Representative data from the B16 model. Ten mice were included in each group, Error bars, SEM, (***P*<0.01, ****P*<0.001).

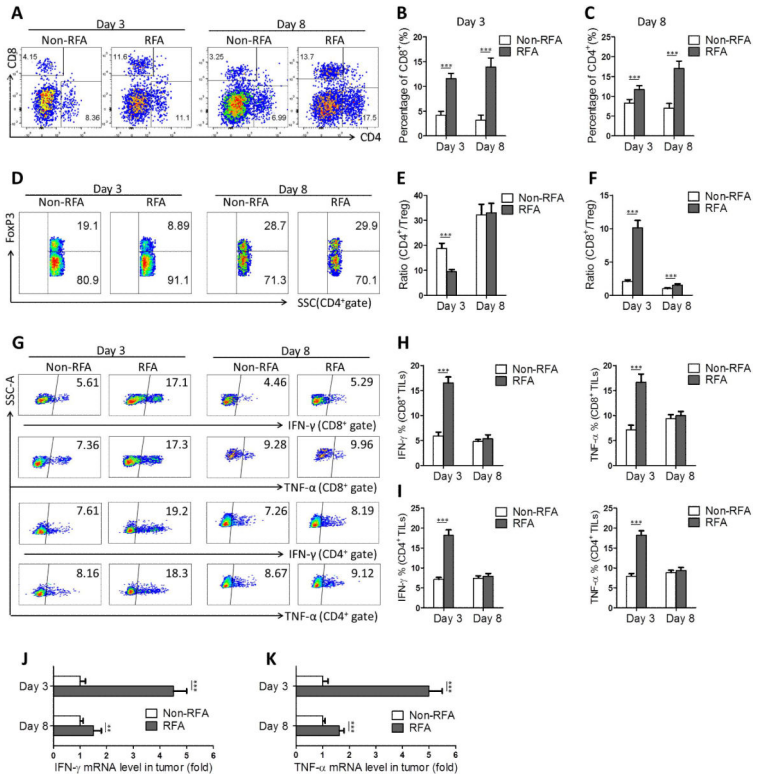

Figure 3. Induction of T cells infiltration into distant tumor after RFA and analysis of their functional status

1×10^6 CT26 cells were injected i.d. into male BALB/C mice on bilateral flanks symmetrically. RFA was administrated as described in Figure 2. On day 3 and 8 after RFA treatment, the tumors on the left flank were resected and either digested to generate single cell suspension or used for RNA isolation. **A** Representative flow cytometric plots showing $CD8^+$and $CD4^+$cells in single cell suspension on day 3 and day 8 after RFA. **B** The percentage of $CD8^+$TIL on day 3 and 8. **C** The percentage of $CD4^+$ cells on day 3 and 8. **D** Flow cytometric plots showing $CD4^+FoxP3^+$Treg. **E** Percentages of $FoxP3^+$ within $CD4^+$ TIL. **F** $CD8^+$ to Treg ratio. **G** Representative flow cytometric plots showing IFN-γ and TNF-α expression on $CD8^+$ and $CD4^+$TIL. **H** percentages of IFN-γ^+ and TNF-α^+ within $CD8^+$TIL. **I** percentages of IFN-γ^+ and TNF-α^+ within $CD4^+$TIL. **J** The IFN-γ mRNA level in total tumor tissue analyzed by RT-QPCR on day 3 and 8. **K** The TNF-α mRNA level in total tumor tissue. Each data point represents cumulative results from two independent experiments with 5 mice per group (values represent means±SEM, ***P<0.001).

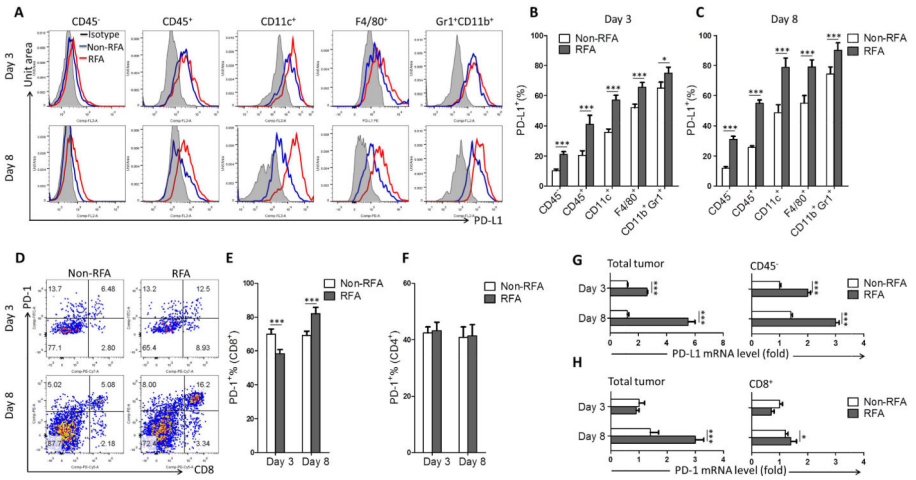

Figure 4. PD-L1/PD-1 expression in the distant tumor after RFA treatment in the CT26 tumor-bearing mice

The CT26 tumor bearing mice models were established and treated as described in Figure 3. **A** Representative flow cytometric histograms showing PD-L1 expression on tumor and stromal cells ($CD45^-$), total infiltrating immune cells ($CD45^+$), dendritic cells ($CD11c^+$), macrophages ($F4/80^+$) and MDSCs ($Gr1^+CD11b^+$) in contralateral tumor on day 3 and 8 after RFA. **B** Percentages of $PD\text{-}L1^+$ cells on day 3 upon RFA. **C** Percentages of $PD\text{-}L1^+$ cells on day 8. **D** Representative flow cytometric plots showing PD-1 expression on $CD8^+$ cells within $CD45^+$ population on day 3 and 8. **E** Percentages of $PD\text{-}1^+$cells within $CD8^+$TIL. **F** Percentage of $PD\text{-}1^+$ cells within $CD4^+$ cells. **G** The PD-L1 mRNA level in total tumor (left panel) and isolated $CD45^-$ cells (right panel). **H** The PD-1 mRNA level in total tumor (left panel) and isolated $CD8^+$TIL (right panel). Data represent cumulative results from two independent experiments with 5 mice per group (values represent means ±SEM,*P<0.05, **P<0.01, ***P<0.001).

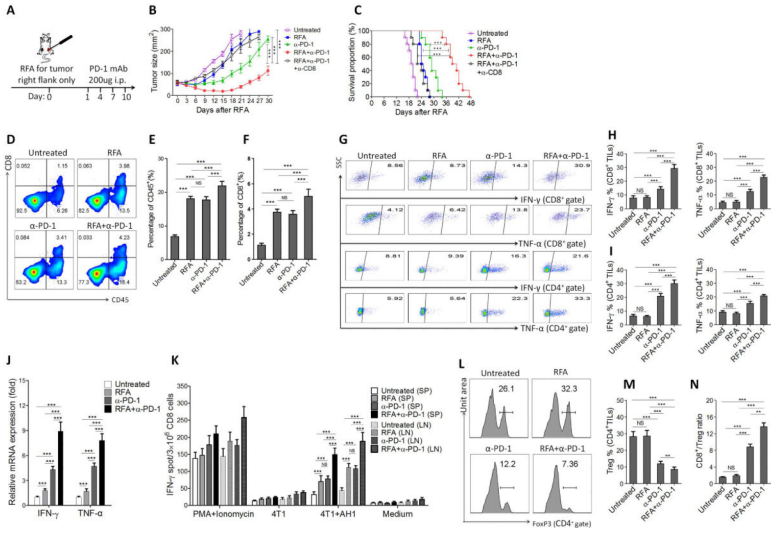

Figure 5. RFA and the anti-PD-1 therapy synergistically enhanced T cell-mediated antitumor immunity

A Schematic drawing of the study. The CT26 tumor-bearing mice models were established and treated with RFA as described in Figure 2. Anti-PD-1 mAbs was administered i.p. to mice on day 1 after RFA, and subsequently once every 3 days for a total of four times. The tumors on the left flank were resected and either digested to generate single cell suspension or used for RNA isolation on day 12. For depletion of $CD8^+$ T cells, 250 μg CD8 mAbs were injected i.p. starting from 1 day before RFA and subsequently once every 3 days for a total of four times. **B** The size of the tumors on the left flank was monitored every three days after RFA (ten mice in each group). **C** Kaplan-Meier survival curves are shown and the log-rank test was performed. **D** Representative flow cytometric plots showing $CD8^+$and $CD45^+$ cells in single cell suspension on day 12 after RFA. **E** Percentages of $CD45^+$ cells within single cell suspension. **F** Percentages of $CD8^+$TIL. **G** Representative flow cytometric plots of IFN-γ and TNF-α expressing $CD8^+$ and $CD4^+$TIL. **H** Percentages of IFN-γ^+ and TNF-α^+ within $CD8^+$TIL. **I** Percentages of IFN-γ^+ and TNF-α^+ within $CD4^+$TIL. **J** The mRNA level of IFN-γ and TNF-α in tumor tissues analyzed by RT-QPCR. **K** Detection of IFN-γ secretion by $CD8^+$T cells in the spleens (SP) and draining lymph nodes (LN) in response to AH1 peptide by ELISPOT. **L** Representative flow cytometric histogram showing $CD4^+$ $FoxP3^+$Treg. **M** Percentages of $FoxP3^+$ within $CD4^+$ TIL. **N** $CD8^+$ to Treg ratio. Data represent results from 1 of 2 independent experiments with 5 mice per group (values represent means±SEM, **P*<0.01, **P<0.05, ****P*<0.001).

Table 1

Analysis of the IHC staining of CD8 and CD4 in matched endoscopic biopsy (EB) and resected tumor (RT) specimens

	Endoscopic biopsy			Resected tumor		
	Non-RFA N (%)	**RFA n(%)**	***P* value**	**Non-RFA n(%)**	**RFA n(%)**	***P* value**
CD8			0.268			<0.001
<10	12(30.0)	10(26.3)		14(35.0)	2(5.3)	
10-20	9(22.5)	10(26.3)		9(22.5)	7(18.4)	
21-40	12(30.0)	12(31.6)		11(27.5)	15(39.5)	
>40	7(17.5)	6(15.8)		6(15.0)	14(36.8)	
CD4			0.812			0.001
<10	8(20.0)	7(18.5)		9(22.5)	4(10.5)	
10-20	10(25.0)	11(28.9)		11(27.5)	7(18.5)	
21-40	13(32.5)	10(26.3)		12(30.0)	14(36.8)	
>40	9(22.5)	10(26.3)		8(20.0)	13(34.2)	
CD8:CD4 ratio			1.000			0.007
≤1	23(57.5)	22(52.6)		25(62.5)	12(34.2)	
>1	17(42.5)	16(47.4)		15(37.5)	26(65.8)	